LANGMUIR
Article
Cite This: *Langmuir* 2018, 34, 3030−3036
pubs.acs.org/Langmuir

Emergence of Droplets at the Nonequilibrium All-Aqueous Interface in a Vertical Hele-Shaw Cell

Youchuang Chao,[†,‡] Sze Yi Mak,[†,‡] Qingming Ma,[†,‡] Jing Wu,[†,‡] Zijing Ding,[†,∥] Lei Xu,[§] and Ho Cheung Shum*[,†,‡]

[†]Department of Mechanical Engineering, The University of Hong Kong, Pokfulam Road, Hong Kong, China
[‡]HKU-Shenzhen Institute of Research and Innovation (HKU-SIRI), Shenzhen, Guangdong 518000, China
[§]Department of Physics, The Chinese University of Hong Kong, Hong Kong, China

Supporting Information

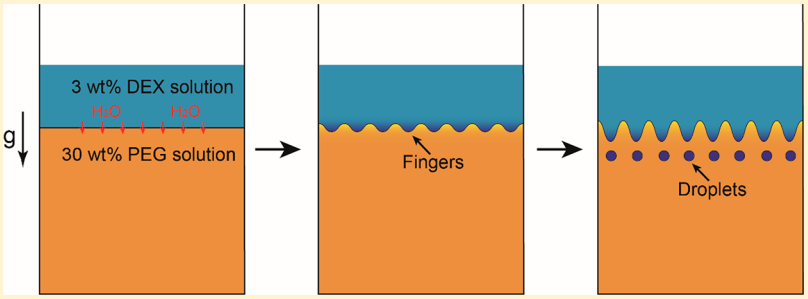

ABSTRACT: The interfacial phenomena at liquid−liquid interfaces remain the subject of constant fascination in science and technology. Here, we show that fingers forming at the interface of nonequilibrium all-aqueous systems can spontaneously break into an array of droplets. The dynamic formation of droplets at the water−water (w/w) interface is observed when a less dense aqueous phase, for instance, the dextran solution, is placed on a denser aqueous phase, the polyethylene glycol solution, in a vertical Hele-Shaw cell. Because of the gradual diffusion of water from the upper phase into the lower phase, a dense layer appears at the nonequilibrium w/w interface. As a result, a periodic array of fingers emerge and sink. Remarkably, these fingers break up and an array of droplets are emitted from the interface. We characterize the wavelength of fingering by measuring the average distance between the dominant fingers. By varying the initial concentrations of the two nonequilibrium aqueous phases, we identify experimentally a phase diagram with a wide parameter space in which finger breaking occurs. Finally, plenty of droplets, spontaneously formed when one phase is continuously deposited onto another aqueous phase, further confirm the robustness of our experimental results. Our work suggests a simple yet efficient approach with a potential upscalability to generate all-aqueous droplets.

INTRODUCTION

When a denser fluid is placed on top of a less dense one in the gravitational field, the fingering phenomenon often arises because of the density-driven instability at the interface, known as the Rayleigh−Taylor (RT) instability.[1−3] Another classic instability driven by density is the double diffusive (DD) instability when solutions of two solutes with different rates of diffusion come into contact.[4] These instabilities occur widely in nature and modern multiphase fluid technology, such as in star formation,[5] sediment transport,[6,7] geologic CO_2 sequestration,[8,9] and inertial confinement fusion.[10] The classical density-driven instability of two-layer systems in the vertical Hele-Shaw (HS) geometry has been intensively studied. For instance, in immiscible systems, the density difference drives the instability, whereas the interfacial tension provides a stabilizing effect, and in miscible two-layer systems, molecular diffusion also contributes to stabilizing the system, similar to interfacial tension.[11,12] In contrast, the fingering instability in complex systems is much less understood, despite its relevance to many practical applications. Recently, it has been shown that, by introducing the chemical reactions in partially miscible systems, the onset of the convection dissolution can be controlled.[13−16] For instance, in the carbon dioxide (CO_2) sequestration, if sodium hydroxide (NaOH) is added into the lower aqueous layer, the growth rate of the convection could increase because of the modification of the density profile.[16] Another example is found in the sediment transport, where uniform sediments are always present because the irregularly shaped particles tend to laterally align with gravity, smoothing out the instability induced by density fluctuation.[17] More recently, the systems of nonequilibrium ternary mixtures are of particular interest because of their spontaneous phase-separation behavior.[18−22] For instance, high-order multiple emulsions are successfully fabricated by the mass-transfer-induced phase separation of ternary mixtures.[21,22] However,

Received: December 7, 2017
Revised: January 21, 2018
Published: February 21, 2018

DOI: 10.1021/acs.langmuir.7b04168
Langmuir 2018, 34, 3030−3036

the density-driven instability, in such ternary systems involving mass-transfer-induced phase separation, has not yet been explored.

In this paper, we experimentally study the fingering instability at the interface of a typical nonequilibrium ternary system, the all-aqueous system,[23−25] mainly inside a vertically orientated HS cell. The upper and lower layers of the HS cell are made up of two out-of-equilibrium aqueous solutions, typically, a less dense dextran (DEX) solution and a denser polyethylene glycol (PEG) solution.[26] We find that the fingering instability occurs at the water−water (w/w) interface because a denser layer is formed as a result of water diffusion from the DEX phase to the PEG phase. Surprisingly, during the fingering, the unstable fingers break into regular droplets. By measuring the mean wavelength of the instability at the interface, we show how the initial concentrations of DEX and PEG solutions affect the interfacial instability. In addition, we find that for different initial concentrations, two qualitatively different regimes, here called RT-type fingering without droplet formation and DD-type fingering with droplet formation, are identified. Furthermore, we present a phase diagram that delineates the range of initial concentrations, within which the fingers could break into droplets. Finally, droplets spontaneously formed when one aqueous solution is continuously deposited onto another bulk aqueous phase, further confirming the validity of our experimental results. Our work yields new insights into the interfacial phenomena in nonequilibrium all-aqueous systems.

In addition, our results will facilitate efficient fabrication of all-aqueous emulsion droplets, which have great potential in drug and cell delivery applications because of their all-aqueous nature.[27,28] Traditional methods including inhomogeneous extensional and shear flow to produce emulsion droplets contribute to a wide-size distribution.[29] Although recent methods, such as microfluidics, have been proposed to fabricate all-aqueous droplets, the production frequency is very low.[30−32] This low production rate mainly comes from the slow dynamics because of the ultralow interfacial tension of all-aqueous interface (less than 10^{-2} to 1 mN/m[33−36]), resulting in a slow breakup of liquid jets that relies on Rayleigh−Plateau mechanism in microfluidics.[37] Therefore, the formation of all-aqueous emulsion droplets simply by spontaneous breakup of liquid fingers at the nonequilibrium w/w interface provides a viable and efficient alternative for all-aqueous emulsification.

EXPERIMENTAL SECTION

Chemicals. Polyethylene glycol (PEG, molecular weight M_w = 8 kDa) and PEG (M_w = 6 kDa) are purchased from Aladdin, Shanghai, China; DEX (M_w = 500 kDa) and DEX (M_w = 10 kDa) are purchased from CASB, Shanghai, China. The PEG and DEX are used to prepare the two aqueous phases. Methylene blue, used to enhance the optical contrast, is purchased from Sigma-Aldrich, St. Louis, USA.

Fabrication of HS Cell. The HS cell[38,39] consists of two parallel glass plates (76 × 52 × 1 mm), which are separated by poly(methyl methacrylate) (PMMA) shims or glass capillaries. The glass plates are cleaned in an acetone solution in the ultrasonic bath for 15 min, sonicated in ethanol solution for 15 min, and then rinsed with deionized water, and finally dried in the oven.[40] The thickness of the HS cells are varied by adopting different thickness of PMMA shims or different diameter of glass capillaries, which ranges from 0.4 to 4.2 mm and are measured by a vernier caliper. The edges of the HS cell are sealed with epoxy.

Experiments in HS Cell. The experimental setup for observing the interfacial phenomena at the nonequilibrium all-aqueous interface is illustrated in Figure 1. The upper and lower layers of the vertically orientated HS cell are initially filled with DEX (molecular weight M_w = 500 kDa, 1−30 wt %) or DEX (molecular weight M_w = 10 kDa, 5 wt %) solutions and a denser PEG (molecular weight M_w = 8 kDa, 0−40 wt %) or PEG (molecular weight M_w = 6 kDa, 30 wt %) solutions, respectively. The two phases are separated by a thin lamina with a maximum thickness of 1 mm before contact. After carefully removing the lamina, the development of the flow is recorded by a long-range camera (Nikon D5200) from one side (6000 × 4000 pixels), with a backlighting from a light-emitting diode (LED) panel. The removal of the lamina produces a delay contact of interface much smaller than the time scale of the instability, and this effect could be neglected.[12] Therefore, we assume that the small perturbation induced by the removal of the thin lamina has little influence on the following measurement. The captured images are processed using ImageJ software.

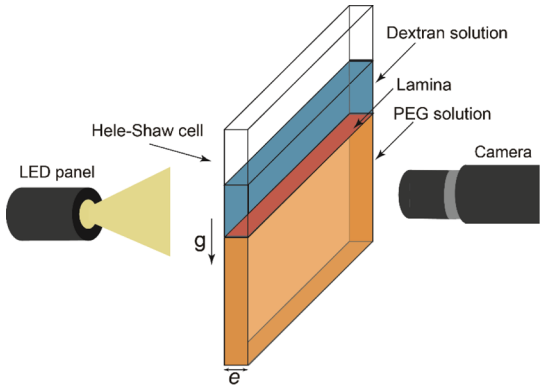

Figure 1. Schematic of the experimental setup. DEX (molecular weight M_w = 500 kDa) and PEG (molecular weight M_w = 8 kDa) aqueous solutions are injected into the upper and lower sections of the HS cell, respectively; the experiments are recorded by the camera with an LED panel backlighting. The upper and lower parts of the cell are separated by a lamina with a maximum thickness of 1 mm before the two phases contact (marked in red color). The removal of the lamina produces a delay contact of interface much smaller than the time scale of the instability, and this effect could be neglected.[12]

Measurement of Density, Viscosity, and Osmolality. The density ρ, osmolality π, and viscosity μ of all-aqueous solutions are measured by a density meter (DA-100M, Mettler Toledo), an osmometer (model 3320, Advanced Instruments), and a viscometer (RheoSense μVISC), respectively. The average values and errors are obtained from three independent experimental runs. All of the values are measured at room temperature (~25 °C).

RESULTS AND DISCUSSIONS

Emergence of Droplets at the Nonequilibrium All-Aqueous Interface. In a typical experiment, we first fill the upper and lower layers of the HS cell with a less dense DEX (M_w = 500 kDa) solution at low concentrations and a denser PEG (M_w = 8 kDa) solution at high concentrations, respectively. After the two phases come into contact, we record the behavior of this all-aqueous (w/w) interface. A typical result and a schematic illustration of the whole destabilization process for a 3 wt % DEX solution being placed on the top of a 30 wt % PEG solution are shown in Figure 2a,b, respectively. Because the two phases are highly out-of-equilibrium, water (M_w = 18 Da) diffuses fast from the DEX phase (osmolality π_{DEX} = 2.7 mOsm/kg·H_2O) to the PEG phase (osmolality π_{PEG} = 1605 mOsm/kg·H_2O). Initially, the density of the 3 wt % DEX phase (ρ_{DEX} = 1.008 g/cm^3) is smaller than the density of the 30 wt % PEG phase (ρ_{PEG} = 1.050 g/cm^3). After a period of diffusion, we find that a denser layer forms at the DEX/PEG interface which becomes unstable and gradually grows into downward fingers.[41,42] Remarkably, we observe that during the process of fingering evolution, all fingers break into droplets (Figure 2a and Movie S1 in the Supporting

DOI: 10.1021/acs.langmuir.7b04168
Langmuir 2018, 34, 3030−3036

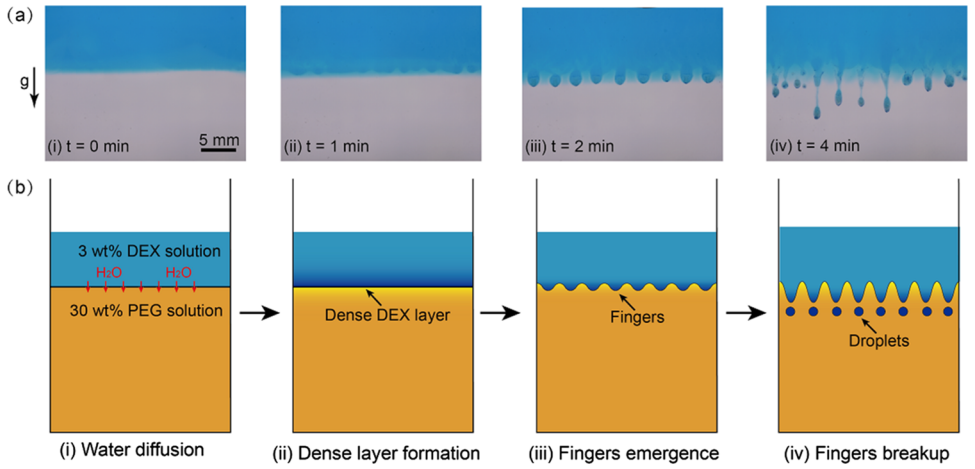

Figure 2. Emergence of droplets at the nonequilibrium all-aqueous interface. (a) Typical snapshots for the time evolution of the whole destabilization process. (b) Schematic illustration of the whole destabilization process. Pure water diffusion and formation of a dense layer (i–ii, stage I); fingering emergence (iii, stage II); and fingers breaking into droplets (iv, stage III). The concentrations of DEX and PEG solutions are 3 and 30 wt %, respectively. The thickness of the HS cell is 1.05 mm. Methylene blue is added to enhance the optical contrast, where in all experiments, the dye concentration is 0.003 wt %. By comparing the experiments with and without dyes, we verify that no noticeable modification is introduced by the dyes. The scale bar is 5 mm.

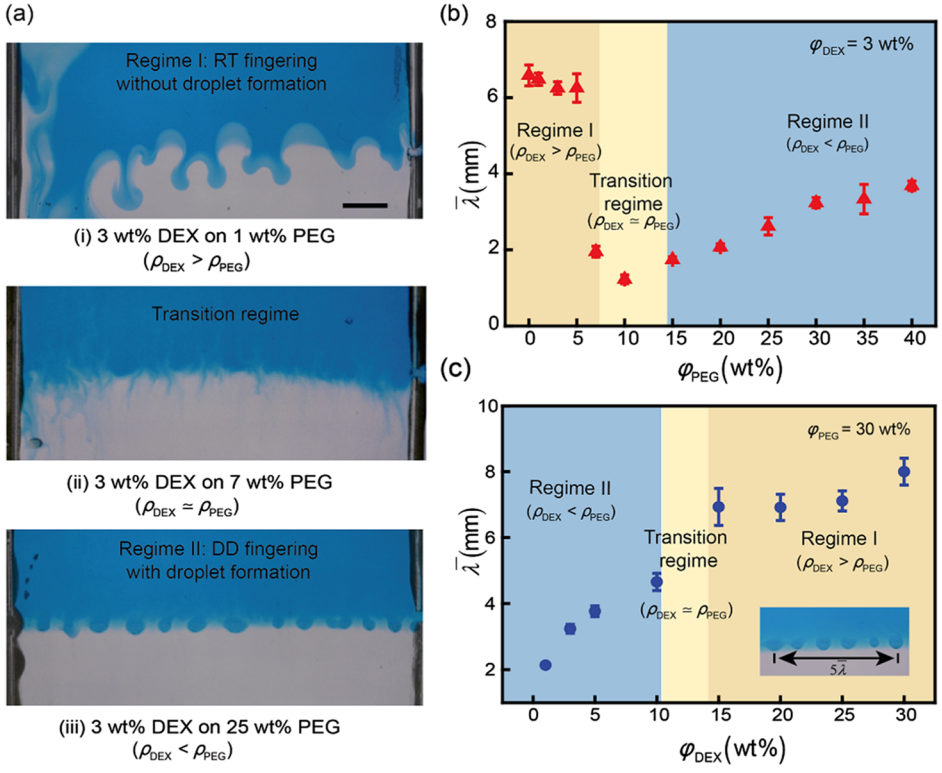

Figure 3. Two typical regimes characterizing the fingering phenomena. (a) Regime I: At small ϕ_{PEG}, fingering instability is the RT-type instability, in which the fingers only grow downward without the formation of droplets ($\rho_{DEX} > \rho_{PEG}$); regime II: At high ϕ_{PEG}, fingering instability is the DD-type instability, in which the fingers could break into droplets ($\rho_{DEX} < \rho_{PEG}$). The transition regime (light yellow, $\Delta\rho \cong 0$) between regime I and regime II is also plotted. (b) Mean wavelength $\bar{\lambda}$ of the observed instability for different initial PEG concentration ϕ_{PEG} with a given DEX concentration ϕ_{DEX} = 3 wt %. (c) Mean wavelength $\bar{\lambda}$ of the observed instability for the different initial DEX concentration ϕ_{DEX} with a given PEG concentration ϕ_{PEG} = 30 wt %. The thickness of the HS cell is 1.05 mm. The inset of (c) shows the method to quantify the mean wavelength of instability, defined as the average distance between peaks of the dominated finger beneath the interface. Each point is obtained from three independent runs performed in the same condition. The scale bar is 5 mm.

Information). The important role of water diffusion from the top phase to the bottom phase is further supported by a control experiment, where no droplets are observed when the top phase has a lower density but a higher osmolality than those of the bottom phase (see Figure S1 in the Supporting Information).

The evolution of the nonequilibrium w/w interface can be generally classified into three stages. Initially, no fingering instability is present at the interface. As the water in the DEX phase gradually diffuses into the PEG phase, a dense DEX layer is observed (stage I, Figure 2a(i,ii),b(i,ii)). At t = 1 min, the fingering instability appears and keeps growing until the fingers

DOI: 10.1021/acs.langmuir.7b04168
Langmuir 2018, 34, 3030–3036

start breaking up at t = 4 min (stage II, Figure 2a(ii,iii),b(ii,iii)). Eventually, the tips of the fingers sink, stretch, and break into droplets (stage III, Figure 2a(iv),b(iv)). In the last stage, we suggest that the tips are exposed into the lower layer with a high concentration; thus, they are dehydrated more drastically than the root parts. With a high dehydration rate, these finger tips possess a high density and sink to the bottom of the HS cell. This observation is also supported by the darker color because of the increased dye concentration at the finger tips, as shown in the recorded images (Figure 2a). As we observe, during the whole destabilization, the nonlinear regime, normally in the form of convective mixing, occurring in classical RT-type and DD-type instabilities, is not observed.[41−43] Instead, all of the fingers spontaneously break into droplets. This interesting result may come from the important role of local diffusion at the finger roots.[43] More likely, during the fingering process, interfaces are formed between the finger phase and the bulk phase as a result of phase separation,[44,45] and thus these fingers break up similar to water dripping from the faucet[46] (see Figure 2a,b; Movie S1 in the Supporting Information).

Two Qualitatively Different Regimes. To quantify the concentration effect on the unstable fingers, we perform experiments with different initial concentration of PEG solution ϕ_{PEG}. A variety of initial concentrations ϕ_{PEG} from 0 to 40 wt % are adopted for a given initial concentration of DEX solution ϕ_{DEX} = 3 wt %. To characterize the fingering phenomenon, we define the mean wavelength, $\bar{\lambda}$, as the average distance between the dominant fingers (see inset of Figure 3c). We find that, for low ϕ_{PEG}, the fingering instability behaves as the RT-type instability without the formation of droplets, as shown in Figure 3a(i). The RT-type instability is caused by the higher initial density of DEX solution in the upper layer than that of PEG solution in the lower layer (see Tables S1 and S2 in the Supporting Information). In this regime, the mean dominant wavelength of the fingers $\bar{\lambda}$ is around six times the gap width e, close to 5 ± 1 obtained in the previous experimental and numerical study,[12] as shown in Figure 3b. As for high concentration of PEG solution, the initial density of DEX solution is lower than that of PEG solution in the lower layer, the fingering instability resembles the DD-type instability but with the formation of droplets (Figure 3a(iii)). In addition, a transition regime is presumably present (Figure 3a(ii)). The mean wavelength strongly depends on the ϕ_{PEG} in the DD-type regime. The critical concentration ϕ_{PC}, representing the transition from RT-type instability to DD-type instability, is around 7 wt % for a given ϕ_{DEX} = 3 wt %. Besides, we are able to observe the breakup of fingers only if the ϕ_{PEG} is above the critical value ϕ_{PC} (Figure 3a,b; Movies S2−S4 in the Supporting Information). The average size of the resulting droplets, d, strongly depends on the mean wavelength $\bar{\lambda}$ of the fingers and increases with the increasing mean wavelength $\bar{\lambda}$, as shown in Figure S2 in the Supporting Information.

We also observe that, for high ϕ_{PEG} above the critical concentration ϕ_{PC}, some of the fingers merge with their neighbors, whereas afterward emit droplets as well (Movie S4 in the Supporting Information). Although for low ϕ_{PEG} but above the critical concentration ϕ_{PC}, the unstable fingers penetrate into the lower phase with little mergence with their neighbors (Movie S5 in the Supporting Information). The characteristic time scale of the fingering formation varies substantially for different initial concentrations and may depend on the diffusion rate between the two solutions.[47] Furthermore, we also observe that the heavier falling fingers are highly asymmetrical with the lighter rising fingers, which may be caused by the different viscosity of the two aqueous phases.[48]

To test whether these two different types of instability are also present for different concentration of DEX solutions ϕ_{DEX}, we plot the mean wavelength $\bar{\lambda}$ of the observed images as a function of the initial DEX concentration ϕ_{DEX} for a given ϕ_{PEG} = 30 wt %. For a typical variation, $\bar{\lambda}$ increases from 2.1 to 4.6 mm as ϕ_{DEX} increases from 1 to 10 wt %. Indeed, a critical DEX concentration exists, delimiting the RT-type fingering and DD-type fingering, which is indicated by a jump of the fingering wavelength for 10 to 15 wt % DEX solutions, as shown in Figure 3c. Therefore, we find that only if ϕ_{DEX} is below a critical concentration ϕ_{DC}, fingers can break into droplets, whereas for $\phi_{DEX} > \phi_{DC}$, fingers behave as RT-type instability and quickly grow down into the bottom of the container without breaking into droplets, which is similar to the experimental results illustrated in Figure 3a.

Apart from the effects of the initial DEX and PEG concentrations, another important parameter that possibly affects the fingering instability is the thickness of the HS cell e.[38] Here, we focus on the regime of DD-type fingering with droplet formation and conduct experiments with different cell thickness e, varying from 0.4 to 4.2 mm. The initial concentrations of DEX and PEG solution are 3 and 30 wt %, respectively. Interestingly, we find that the mean wavelength does not appreciably depend on the cell thickness e. Instead, the mean wavelength $\bar{\lambda}$ is nearly constant and approximates to 3 mm for different cell thickness e, as shown in Figure S3 in the Supporting Information. Therefore, we hypothesize that, in this ternary system, the dominant length scale of the DD-type fingering is not determined by the cell thickness but might be relevant to the length scale of diffusion.[42] To support this hypothesis, we gently place a thin layer (∼1.5 mm) of 3 wt % DEX solution on a 30 wt % PEG bulk solution and record the dynamics of the droplet formation, including the length and time scales of nucleation, from a top-down view. We notice that the length and time scales in this case are close to the results obtained in the HS cell, further confirming our hypothesis that the dominant length scales are related to diffusion (see Figure S4 in the Supporting Information).

Phase Diagram Delineating Two Different Regimes. To obtain the parameter space within which the droplets could form at the nonequilibrium w/w interface, we study parametrically this fingering phenomena for various combinations of the two aqueous phases. We vary the initial DEX concentration ϕ_{DEX} and PEG concentration ϕ_{PEG} in a large parameter space, with ϕ_{DEX} and ϕ_{PEG} ranging from 1 to 30 wt % and from 0 to 40 wt %, respectively (summary of all density, viscosity, and osmolality are given in Tables S1 and S2 in the Supporting Information). Then, we organize our experimental observations in a ϕ_{PEG}−ϕ_{DEX} phase diagram, as shown in Figure 4.

Generally, the ϕ_{PEG}−ϕ_{DEX} phase diagram delineates the interfacial fingering into two different regimes: RT-type fingering without droplet formation and DD-type fingering with droplet formation (Figure 4). For a small ϕ_{PEG}, the density of DEX solution is larger than the density of PEG solution in which $\rho_{DEX} > \rho_{PEG}$, triggering the RT-type instability (circles in Figure 4). In this region, no droplets are observed because of the fast evolution of the RT-type instability. As we increase the ϕ_{PEG} for a relatively small ϕ_{DEX}, the density of the DEX phase is smaller than the density of the PEG phase in which $\rho_{DEX} < \rho_{PEG}$, and the fingers emerging at the interfacial region become unstable and break into small droplets (triangles in Figure 4). The initial density difference, $\Delta\rho = \rho_{DEX} - \rho_{PEG}$, is assumed to be a critical parameter

DOI: 10.1021/acs.langmuir.7b04168
Langmuir 2018, 34, 3030−3036

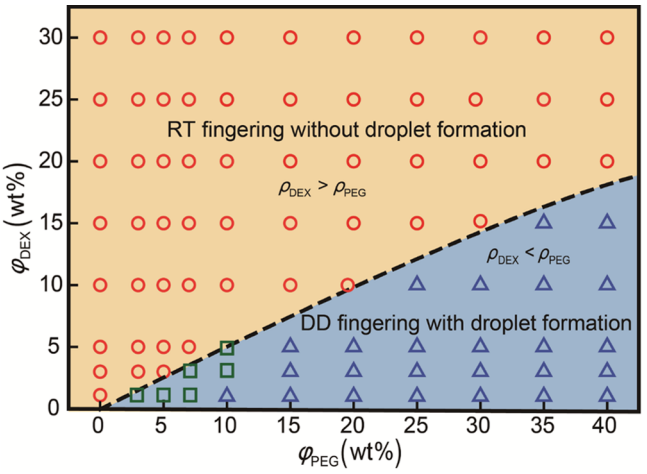

Figure 4. Phase diagram. On the basis of initial DEX concentration ϕ_{DEX} and initial PEG concentration ϕ_{PEG}, two qualitatively different regimes are identified: RT-type fingering without droplet formation where $\rho_{DEX} > \rho_{PEG}$ (circles), and DD-type fingering with droplet formation where $\rho_{DEX} < \rho_{PEG}$ (triangles). Transition points between the two regimes (see Figure 3a(ii)) are found to be near the curve of $\Delta\rho \cong 0$ (squares). The black dashed line, representing the density difference $\Delta\rho \cong 0$, successfully captures the transition between the RT-type fingering and DD-type fingering.

for determining the transition between RT-type instability and DD-type instability. To account for this value, we draw the curve of $\Delta\rho \cong 0$ into the phase diagram. Indeed, this curve captures the boundary between the RT-type fingering and DD-type fingering (dashed line in Figure 4). We find that only in the regime of DD-type fingering, in which $\rho_{DEX} < \rho_{PEG}$, the fingers can break into droplets. The presumable transition points (see Figure 3(ii)) near the curve of $\Delta\rho \cong 0$ are also plotted in Figure 4 (squares). Overall, our phase diagram suggests that a suitable combination of a less dense DEX solution and a denser PEG solution could provide a versatile control to fabricate droplets at the nonequilibrium w/w interface. This self-emergence of droplets is not limited to DEX (M_w = 500 kDa)−PEG (M_w = 8 kDa) aqueous system. The same phenomenon is also observed in DEX (M_w = 10 kDa)−PEG (M_w = 6 kDa) aqueous system (see Figure S5 in the Supporting Information).

Scalable Platform for Generating All-Aqueous Droplets. To further demonstrate the emergence of fingers and their breakup into an array of droplets, we continuously drip the 3 wt % DEX (M_w = 500 kDa) solution onto the 30 wt % PEG (M_w = 8 kDa) bulk solution in a beaker (Figure 5(i)). We observe that a flat interface is formed (Figure 5(ii)), followed by a large number of fingers spontaneously appearing at the w/w interface (Figure 5(iii)). These fingers break into droplets and eventually sink to the bottom of the container, as shown in Figure 5(iv) and Movie S6 in the Supporting Information. Generally, the whole process in this three-dimensional (3D) container is similar to the self-emergence of droplets observed in the confined quasi-two-dimensional (2D) HS geometry (see Figures 5 and 2), further confirming that the self-emergence of the all-aqueous droplets at the nonequilibrium w/w interface could also happen in the 3D configuration. To conclude, with this simple platform, assemblies of all-aqueous droplets could be generated at the nonequilibrium all-aqueous interface with potential upscalability in a very short time (less than 10 min).

Discussions. In this work, we suggest a possible mechanism that accounts for the transition between the regime of RT fingering and the regime of droplet formation. The RT fingering is due to the initially higher density of upper layer than that of lower layer in the vertical HS cell, where we could not observe any droplets. However, when the initial density of the upper layer is smaller than that of the lower layer and the initial osmolality of the top layer is smaller than that of lower layer, the formation of fingers is observed, and the fingers subsequently break up into droplets. The formation of all-aqueous droplets is possibly because of the diffusion of water from the top layer into the lower layer, inducing the formation of a dense layer near the interface. This dense layer is unstable because of the density difference and consequently forms fingers, which then break up into droplets. On the basis of the initial concentrations of DEX and PEG solutions, we summarize all of the experimental results into a phase diagram that clearly shows the transition boundary between the two regimes.

Although our phase diagram clearly delineates two qualitatively different regimes in which the droplet could form or not, our analysis does not describe other details of the experimental results. For instance, the formation of the dense aqueous layer, the process of phase separation, droplet nucleation in all-aqueous systems, the emergence of fingers, and the breakup of the fingers are not yet quantitatively explained. A comprehensive theoretical model or a numerical simulation accounting for the whole process of the self-emergent droplets is beyond the scope of the present work. This experimental discovery will stimulate further theoretical and numerical investigations coupling hydrodynamics, diffusion, phase separation, and gravitational effect. With a simple setup, assemblies of all-aqueous droplets are directly

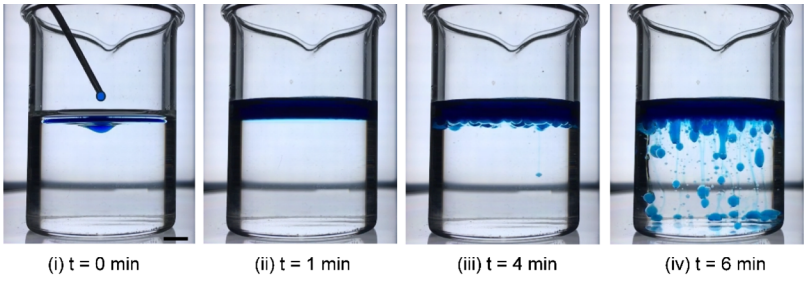

Figure 5. Spontaneous droplet formation at the nonequilibrium w/w interface in a scalable method. Initially, the DEX phase is continuously dripped on the PEG phase (i), then a flat w/w interface is formed (ii), the interface becomes unstable with finger formation (iii), and these fingers break into droplets and finally sink to the bottom of the container (iv). The whole evolution of w/w interface in this 3D cylindrical device (beaker) is similar to the self-emergence of droplets in the 2D vertical HS geometry. The concentrations of DEX and PEG solutions are 3 and 30 wt %, respectively. The scale bar is 5 mm.

DOI: 10.1021/acs.langmuir.7b04168
Langmuir 2018, 34, 3030−3036

emitted at the nonequilibrium all-aqueous interface in the gravitational field, and their size can be easily adjusted by varying the initial concentrations of two nonequilibrium aqueous phases.

CONCLUSIONS

In summary, we have shown the interfacial phenomena of fingering instability at the nonequilibrium all-aqueous interfaces. Our work highlights the role of nonequilibrium effect in all-aqueous systems as a reliable route to produce droplets. The instability observed in our nonequilibrium all-aqueous systems closely resembles those in miscible or partially miscible two-layer systems. However, in this work, using a single all-aqueous system, the RT-type instability and the DD-type instability can be observed with the formed fingers breaking up into regular droplets rather than turning to the nonlinear stage of convective mixing. These droplets can be easily collected and used as templates for synthesizing all-aqueous-based biomaterials. Furthermore, the formation of droplet array by continuously dripping one aqueous phase onto another aqueous phase further confirms the robustness of our experimental results. We believe that our results open up a versatile approach to generate all-aqueous emulsions that possess great potential in practical applications.

ASSOCIATED CONTENT

Supporting Information

The Supporting Information is available free of charge on the ACS Publications website at DOI: 10.1021/acs.langmuir.7b04168.

All density, viscosity, and osmolality of the adopted solutions; control experiment where the top phase has a lower density but a higher osmolality compared to the bottom phase; the relationship between the mean wavelength $\bar{\lambda}$ and the resulting average diameter of the droplets d; the mean wavelength $\bar{\lambda}$ of the fingers for different cell thicknesses e; typical top-down view of a thin layer of 3 wt % DEX solution placed on a 30 wt % PEG bulk solution; the fingering phenomenon in a different all-aqueous system; detailed descriptions of all the Supplemental Movies (PDF)

Emergence of droplets at the nonequilibrium all-aqueous interface in a vertical HS cell (AVI)

RT fingering without droplet formation (Regime I) in a vertical HS cell (AVI)

Transition regime between the RT fingering and DD fingering in a vertical HS cell (AVI)

DD fingering with droplet formation (Regime II) in a vertical HS cell with a PEG concentration of 25 wt% (AVI)

DD fingering with droplet formation (Regime II) in a vertical HS cell with a PEG concentration of 10 wt% (AVI)

Formation of all-aqueous droplets in a simple setup (AVI)

AUTHOR INFORMATION

Corresponding Author

*E-mail: ashum@hku.hk.

ORCID

Youchuang Chao: 0000-0001-8495-786X

Ho Cheung Shum: 0000-0002-6365-8825

Present Address

[‖]Department of Applied Mathematics and Theoretical Physics, Centre for Mathematical Sciences, University of Cambridge, Wilberforce Road, Cambridge CB3 0WA, United Kingdom.

Author Contributions

The manuscript was written through contributions of all authors. All authors have given approval to the final version of the manuscript.

Notes

The authors declare no competing financial interest.

ACKNOWLEDGMENTS

We thank Dr. Alban Sauret and Dr. Tiantian Kong for helpful discussions. This research is supported by the General Research Fund (nos. HKU 719813E, 17304514, 17306315, and 17329516) and the Collaborative Research Fund (C6004-14G) from the Research Grants Council of Hong Kong, the General Program (no. 21476189/B060201), and the Major Research plan (no. 91434202) from the National Natural Science Foundation of China, as well as the Seed Funding Programme for Basic Research (nos. 201411159038 and 201511159280) from the University of Hong Kong.

REFERENCES

(1) Strutt, J.; Rayleigh, L. Investigation of the character of the equilibrium of an incompressible heavy fluid of variable density. *Proc. Lond. Math. Soc.* **1882**, *14*, 170.

(2) Taylor, G. The instability of liquid surfaces when accelerated in a direction perpendicular to their planes. I. *Proc. R. Soc. London, Ser. A* **1950**, *201*, 192.

(3) Lewis, D. J. The instability of liquid surfaces when accelerated in a direction perpendicular to their planes. II. *Proc. R. Soc. London, Ser. A* **1950**, *202*, 81.

(4) Huppert, H. E.; Turner, J. S. Double-diffusive convection. *J. Fluid Mech.* **1981**, *106*, 299−329.

(5) Jiang, Y.-F.; Davis, S. W.; Stone, J. M. Nonlinear evolution of Rayleigh-Taylor instability in a radiation-supported atmosphere. *Astrophys. J.* **2013**, *763*, 102.

(6) Parsons, J. D.; Bush, J. W. M.; Syvitski, J. P. M. Hyperpycnal plume formation from riverine outflows with small sediment concentrations. *Sedimentology* **2001**, *48*, 465−478.

(7) Kneller, B.; Nasr-Azadani, M. M.; Radhakrishnan, S.; Meiburg, E. Long-range sediment transport in the world's oceans by stably stratified turbidity currents. *J. Geophys. Res.: Oceans* **2016**, *121*, 8608.

(8) Lindeberg, E.; Wessel-Berg, D. Vertical convection in an aquifer column under a gas cap of CO_2. *Energy Convers. Manage.* **1997**, *38*, S229−S234.

(9) Emami-Meybodi, H.; Hassanzadeh, H.; Green, C. P.; Ennis-King, J. Convective dissolution of CO_2 in saline aquifers: Progress in modeling and experiments. *Int. J. Greenhouse Gas Control* **2015**, *40*, 238−266.

(10) Kilkenny, J. D.; Glendinning, S. G.; Haan, S. W.; Hammel, B. A.; Lindl, J. D.; Munro, D.; Remington, B. A.; Weber, S. V.; Knauer, J. P.; Verdon, C. P. A review of the ablative stabilization of the Rayleigh−Taylor instability in regimes relevant to inertial confinement fusion. *Phys. Plasmas* **1994**, *1*, 1379−1389.

(11) Homsy, G. M. Viscous fingering in porous media. *Annu. Rev. Fluid Mech.* **1987**, *19*, 271−311.

(12) Fernandez, J.; Kurowski, P.; Petitjeans, P.; Meiburg, E. Density-driven unstable flows of miscible fluids in a Hele-Shaw cell. *J. Fluid Mech.* **2002**, *451*, 239−260.

(13) Citri, O.; Kagan, M. L.; Kosloff, R.; Avnir, D. Evolution of chemically induced unstable density gradients near horizontal reactive interfaces. *Langmuir* **1990**, *6*, 559−564.

(14) Eckert, K.; Grahn, A. Plume and finger regimes driven by an exothermic interfacial reaction. *Phys. Rev. Lett.* **1999**, *82*, 4436.

DOI: 10.1021/acs.langmuir.7b04168
Langmuir 2018, 34, 3030−3036

(15) Budroni, M. A.; Riolfo, L. A.; Lemaigre, L.; Rossi, F.; Rustici, M.; De Wit, A. Chemical control of hydrodynamic instabilities in partially miscible two-layer systems. *J. Phys. Chem. Lett.* **2014**, *5*, 875−881.
(16) Loodts, V.; Thomas, C.; Rongy, L.; De Wit, A. Control of convective dissolution by chemical reactions: general classification and application to CO_2 dissolution in reactive aqueous solutions. *Phys. Rev. Lett.* **2014**, *113*, 114501.
(17) Goldfriend, T.; Diamant, H.; Witten, T. A. Screening, hyperuniformity, and instability in the sedimentation of irregular objects. *Phys. Rev. Lett.* **2017**, *118*, 158005.
(18) Song, Y.; Shum, H. C. Monodisperse w/w/w double emulsion induced by phase separation. *Langmuir* **2012**, *28*, 12054−12059.
(19) Zarzar, L. D.; Sresht, V.; Sletten, E. M.; Kalow, J. A.; Blankschtein, D.; Swager, T. M. Dynamically reconfigurable complex emulsions via tunable interfacial tensions. *Nature* **2015**, *518*, 520−524.
(20) Moon, B.-U.; Hwang, D. K.; Tsai, S. S. H. Shrinking, growing, and bursting: microfluidic equilibrium control of water-in-water droplets. *Lab Chip* **2016**, *16*, 2601−2608.
(21) Liang, S.; Li, J.; Man, J.; Chen, H. Mass-transfer-induced multistep phase separation in emulsion droplets: Toward self-assembly multilayered emulsions and onionlike microspheres. *Langmuir* **2016**, *32*, 7882−7887.
(22) Haase, M. F.; Brujic, J. Tailoring of high-order multiple emulsions by the liquid−liquid phase separation of ternary mixtures. *Angew. Chem., Int. Ed.* **2014**, *53*, 11793−11797.
(23) Song, Y.; Shimanovich, U.; Michaels, T. C.; Ma, Q.; Li, J.; Knowles, T. P.; Shum, H. C. Fabrication of fibrillosomes from droplets stabilized by protein nanofibrils at all-aqueous interfaces. *Nat. Commun.* **2016**, *7*, 12934.
(24) Xue, L.-H.; Xie, C.-Y.; Meng, S.-X.; Bai, R.-X.; Yang, X.; Wang, Y.; Wang, S.; Binks, B. P.; Guo, T.; Meng, T. Polymer−protein conjugate particles with biocatalytic activity for stabilization of water-in-water emulsions. *ACS Macro Lett.* **2017**, *6*, 679−683.
(25) Mak, S. Y.; Chao, Y.; Rahman, S.; Shum, H. C. Droplet formation by rupture of vibration-induced interfacial fingers. *Langmuir* **2018**, *34*, 926−932.
(26) Ma, Q.; Song, Y.; Baier, G.; Holtze, C.; Shum, H. C. Osmo-solidification of all-aqueous emulsion with enhanced preservation of protein activity. *J. Mater. Chem. B* **2016**, *4*, 1213−1218.
(27) Strulson, C. A.; Molden, R. C.; Keating, C. D.; Bevilacqua, P. C. RNA catalysis through compartmentalization. *Nat. Chem.* **2012**, *4*, 941−946.
(28) Song, Y.; Chan, Y. K.; Ma, Q.; Liu, Z.; Shum, H. C. All-aqueous electrosprayed emulsion for templated fabrication of cytocompatible microcapsules. *ACS Appl. Mater. Interfaces* **2015**, *7*, 13925−13933.
(29) Link, D. R.; Anna, S. L.; Weitz, D. A.; Stone, H. A. Geometrically mediated breakup of drops in microfluidic devices. *Phys. Rev. Lett.* **2004**, *92*, 054503.
(30) Moon, B.-U.; Abbasi, N.; Jones, S. G.; Hwang, D. K.; Tsai, S. S. Water-in-water droplets by passive microfluidic flow focusing. *Anal. Chem.* **2016**, *88*, 3982−3989.
(31) Song, Y. S.; Choi, Y. H.; Kim, D. H. Microextraction in a tetrabutylammonium bromide/ammonium sulfate aqueous two-phase system and electrohydrodynamic generation of a micro-droplet. *J. Chromatogr. A* **2007**, *1162*, 180−186.
(32) Sauret, A.; Shum, H. C. Forced generation of simple and double emulsions in all-aqueous systems. *Appl. Phys. Lett.* **2012**, *100*, 154106.
(33) Wu, Y.-T.; Zhu, Z.-Q.; Mei, L.-H. Interfacial tension of poly(ethylene glycol)+ salt+ water systems. *J. Chem. Eng. Data* **1996**, *41*, 1032−1035.
(34) Atefi, E.; Mann, J. A., Jr; Tavana, H. Ultralow interfacial tensions of aqueous two-phase systems measured using drop shape. *Langmuir* **2014**, *30*, 9691−9699.
(35) Vis, M.; Peters, V. F. D.; Blokhuis, E. M.; Lekkerkerker, H. N. W.; Erné, B. H.; Tromp, R. H. Decreased interfacial tension of demixed aqueous polymer solutions due to charge. *Phys. Rev. Lett.* **2015**, *115*, 078303.
(36) Chao, Y.; Mak, S. Y.; Shum, H. C. The transformation dynamics towards equilibrium in non-equilibrium w/w/o double emulsions. *Appl. Phys. Lett.* **2016**, *109*, 181601.
(37) Geschiere, S. D.; Ziemecka, I.; van Steijn, V.; Koper, G. J. M.; van Esch, J. H.; Kreutzer, M. T. Slow growth of the Rayleigh-Plateau instability in aqueous two phase systems. *Biomicrofluidics* **2012**, *6*, 022007.
(38) Backhaus, S.; Turitsyn, K.; Ecke, R. E. Convective instability and mass transport of diffusion layers in a Hele-Shaw geometry. *Phys. Rev. Lett.* **2011**, *106*, 104501.
(39) Hidalgo, J. J.; Fe, J.; Cueto-Felgueroso, L.; Juanes, R. Scaling of convective mixing in porous media. *Phys. Rev. Lett.* **2012**, *109*, 264503.
(40) Kim, H.; Lee, J.; Kim, T.-H.; Kim, H.-Y. Spontaneous Marangoni mixing of miscible liquids at a liquid−liquid−air contact line. *Langmuir* **2015**, *31*, 8726−8731.
(41) Vreme, A.; Nadal, F.; Pouligny, B.; Jeandet, P.; Liger-Belair, G.; Meunier, P. Gravitational instability due to the dissolution of carbon dioxide in a Hele-Shaw cell. *Phys. Rev. Fluids* **2016**, *1*, 064301.
(42) Slim, A. C.; Bandi, M. M.; Miller, J. C.; Mahadevan, L. Dissolution-driven convection in a Hele−Shaw cell. *Phys. Fluids* **2013**, *25*, 024101.
(43) Gopalakrishnan, S. S.; Carballido-Landeira, J.; De Wit, A.; Knaepen, B. Relative role of convective and diffusive mixing in the miscible Rayleigh-Taylor instability in porous media. *Phys. Rev. Fluids* **2017**, *2*, 012501.
(44) Tan, H.; Diddens, C.; Lv, P.; Kuerten, J. G. M.; Zhang, X.; Lohse, D. Evaporation-triggered microdroplet nucleation and the four life phases of an evaporating Ouzo drop. *Proc. Natl. Acad. Sci. U.S.A.* **2016**, *113*, 8642−8647.
(45) Lamorgese, A.; Mauri, R. Diffusion-driven dissolution or growth of a liquid drop embedded in a continuous phase of another liquid via phase-field ternary mixture model. *Langmuir* **2017**, *33*, 13125−13132.
(46) Ambravaneswaran, B.; Subramani, H. J.; Phillips, S. D.; Basaran, O. A. Dripping-jetting transitions in a dripping faucet. *Phys. Rev. Lett.* **2004**, *93*, 034501.
(47) Riaz, A.; Hesse, M.; Tchelepi, H. A.; Orr, F. M. Onset of convection in a gravitationally unstable diffusive boundary layer in porous media. *J. Fluid Mech.* **2006**, *548*, 87−111.
(48) Tryggvason, G.; Aref, H. Numerical experiments on Hele Shaw flow with a sharp interface. *J. Fluid Mech.* **1983**, *136*, 1−30.

DOI: 10.1021/acs.langmuir.7b04168
Langmuir 2018, 34, 3030−3036